

Direct Electro spray Printing of Gradient Refractive Index Chalcogenide Glass Films

Spencer Novak,^{*,†,‡,§,||} Pao Tai Lin,^{⊥,||} Cheng Li,[‡] Chatdanai Lumdee,[‡] Juejun Hu,^{||} Anuradha Agarwal,^{||} Pieter G. Kik,[‡] Weiwei Deng,[∇] and Kathleen Richardson^{*,‡}

[†]Department of Materials Science and Engineering, School of Engineering and Science, Clemson University, 161 Surrin Hall Clemson, South Carolina 29634, United States

[‡]CREOL, The College of Optics and Photonics, University of Central Florida, 4304 Scorpius Street, Orlando, Florida 32816, United States

[⊥]Department of Electrical and Computer Engineering and Department of Materials Science and Engineering, Texas A&M University, 3128 TAMU, 188 Bizzell Street, College Station, Texas 77843, United States

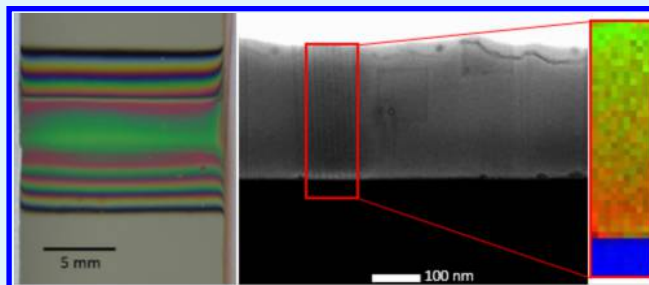
^{||}Microphotonics Center, Massachusetts Institute of Technology, Room 13-4118, 77 Massachusetts Avenue, Cambridge, Massachusetts 02139-4307, United States

^{||}Microphotonics Center and Department of Materials Science and Engineering, Massachusetts Institute of Technology, Room 13-4126, 77 Massachusetts Avenue, Cambridge, Massachusetts 02139-4307, United States

[∇]Department of Mechanical Engineering, Virginia Polytechnic Institute and State University, 635 Price Fork Road, Blacksburg, Virginia 24061, United States

ABSTRACT: A spatially varying effective refractive index gradient using chalcogenide glass layers is printed on a silicon wafer using an optimized electro spray (ES) deposition process. Using solution-derived glass precursors, IR-transparent $\text{Ge}_{23}\text{Sb}_7\text{S}_{70}$ and $\text{As}_{40}\text{S}_{60}$ glass films of programmed thickness are fabricated to yield a bilayer structure, resulting in an effective gradient refractive index (GRIN) film. Optical and compositional analysis tools confirm the optical and physical nature of the gradient in the resulting high-optical-quality films, demonstrating the power of direct printing of multi-material structures compatible with planar photonic fabrication protocols. The potential application of such tailorable materials and structures as they relate to the enhancement of sensitivity in chalcogenide glass based planar chemical sensor device design is presented. This method, applicable to a broad cross section of glass compositions, shows promise in directly depositing GRIN films with tunable refractive index profiles for bulk and planar optical components and devices.

KEYWORDS: gradient refractive index, chalcogenide glass, thin films, electro spray, microphotonics



INTRODUCTION

Mid-IR microphotonics based on chalcogenide glasses (ChGs) have seen significant growth in the past decade. Interest in such materials is largely due to the broad glass-forming region of many ChGs allowing the use of compositional tuning to tailor specific optical properties, such as the refractive index of a photonic structure (waveguide, resonator, filter, etc.). Such tailorability allows the optical design of compact, high contrast structures, and their expanding use has been shown to be compatible with complementary metal–oxide–semiconductor fabrication methods and diverse substrates. Efforts by our team and others have specifically investigated applications such as chip-based chemical or biological sensors based on the integration of light sources, resonator arrays, and detectors.^{1–5}

Current research efforts target the development of low-cost, deployable, highly sensitive devices that identify a chemical by its optical fingerprint, which generally lies in the 3–5 μm

wavelength range, where ChGs have good transparency.⁶ For the probing of analytes with multiple absorption wavelengths or a mixed stream of multiple analytes, it is highly desirable for the on-chip resonators to have a range of resonant wavelengths as well as a broad spectral window of transparency.⁷ According to eq 1, the resonant wavelength, λ_m , of a circular resonator's mode varies with its radius, r , and effective refractive index, $n_{\text{eff},m}$, which is determined by the index of the waveguiding material as well as that of the surrounding material, where m is the mode number.

$$2\pi r n_{\text{eff}} = m \lambda_m \quad (1)$$

Received: May 2, 2017

Accepted: July 19, 2017

Published: July 19, 2017

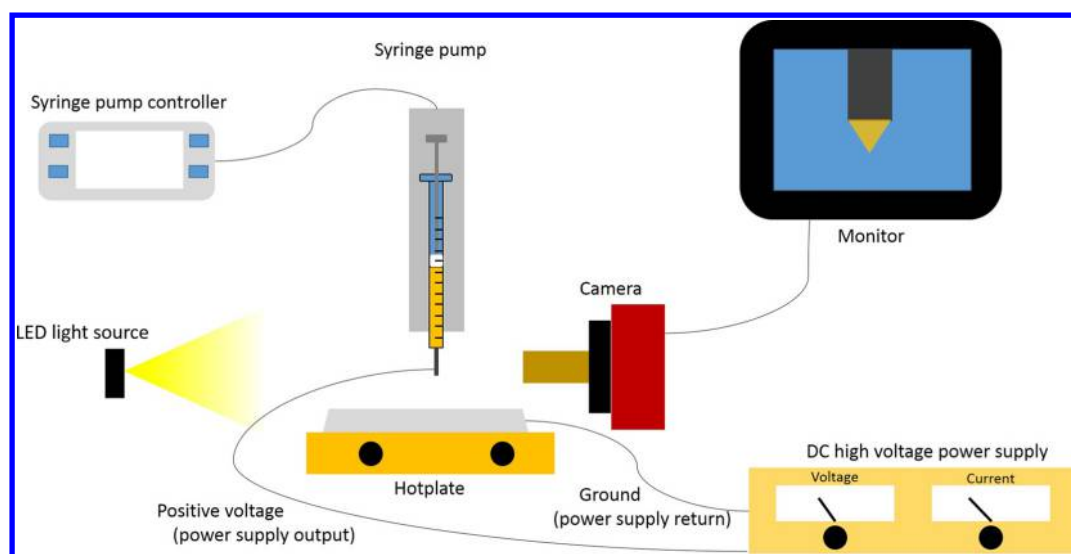


Figure 1. Schematic representation of the main components of the ES system.

This equation results in a dense spectrum of sharp resonances separated by the free spectral range of the resonator. In order to achieve a near-continuous spectrum for probing diverse analytes or mixtures, variation in λ_m has been achieved by varying the size of the resonator, although this can make fabrication more complex and cause deviation of the designed resonant wavelength.^{8,9} In most sensing applications, the use of multiple (identical) resonators reduces the frequency of false positives during a sensing event.

These applications have used single ChG materials with fixed refractive indexes. As noted above, the film indexes in these compositions are tunable with compositional modification. Even greater optical design flexibility could be enabled by the deposition of a gradient refractive index (GRIN) coating over an array of resonators. This would allow a smoother spectral response for a fixed fabrication geometry but requires strict spatial control of the glass composition and glass film attributes including transmission/loss and film thickness. This design flexibility also benefits free-space optical systems. Specifically, IR-transparent GRIN coatings on bulk IR optical components would enable greater design freedom, lower manufacturing costs where aspheric optics are no longer required, and smaller and lightweight optical systems. GRIN coatings based on nanocrystallized optical composites have already been demonstrated in the mid-IR in structures where a low-absorption, high-refractive-index secondary crystalline phase is nucleated and grown within a lower index base glass.¹⁰ This results in an effective index, n_{eff} defined spatially by the laser write beam used to stimulate nanocrystal nucleation, only in the exposed region. Subsequent thermal growth defines the nanocrystallite size and the magnitude and contrast between the modified (increased n_{eff}) regions and the unexposed base glass regions. Here, heat treatment of the unexposed region does not impart any index modification, thus resulting in either a stepwise or a gradient n_{eff} variation when a spatial variation in the laser exposure dose is employed.

In the present effort, the resulting GRIN is realized by spatial control of the thicknesses of the fixed-refractive-index glass layers. Electro spray (ES) deposition offers advantages over the dip or spin coating of solutions in that there is very little waste of material, the process is compatible with roll-to-roll processing, and it is suitable for scale-up.¹¹ The initial studies

on the ES deposition of ChG films have demonstrated that it is feasible to obtain smooth, low-loss films with good IR transparency and controlled thickness profiles realized through controlled relative motion between the nozzle and substrate.^{12,13} In this study, we demonstrate the viability of this approach and report the direct printing of mid-IR-transparent GRIN films achieved by the sequential deposition of two ChG compositions, $\text{Ge}_{23}\text{Sb}_7\text{S}_{70}$ and $\text{As}_{40}\text{S}_{60}$.

EXPERIMENTAL SECTION

Bulk $\text{As}_{40}\text{S}_{60}$ and $\text{Ge}_{23}\text{Sb}_7\text{S}_{70}$ glasses were fabricated by the traditional melt-quenching techniques described elsewhere.¹⁴ High-purity, elemental starting materials were batched into a fused SiO_2 ampule inside a nitrogen-purged glovebox, and the ampule was then sealed under a vacuum with a gas–oxygen torch. The sealed batch was then melted overnight in a rocking furnace to ensure homogeneity, at temperatures of 750 °C for $\text{As}_{40}\text{S}_{60}$ and 850 °C for $\text{Ge}_{23}\text{Sb}_7\text{S}_{70}$. The melts were air-quenched and annealed overnight at temperatures of 150 °C for $\text{As}_{40}\text{S}_{60}$ and 270 °C for $\text{Ge}_{23}\text{Sb}_7\text{S}_{70}$.

Solutions of ChG were realized by the dissolution of these parent glasses in suitable solvents using methodologies discussed elsewhere.^{15–17} The bulk glasses were crushed into powders and dissolved at a concentration of 0.05 g mL⁻¹ in ethanolamine. To expedite dissolution, the mixtures were placed on a hot plate with a surface temperature of about 50 °C. Complete dissolution typically required about 24 h. The solutions were filtered through a 0.45 μm poly(tetrafluoroethylene) filter to remove any large precipitates.

The ES system, schematically illustrated in Figure 1 and discussed in more detail elsewhere, consists of a syringe pump oriented vertically.¹³ The syringe pump head was attached to a desktop computer numerical control machine, which enables the syringe to move along a preprogrammed path over the substrate during deposition. This programmed profile defines the ES cone's dwell time over the substrate that dictates the resulting film thickness.

ChG solution was drawn into a 50 μL Hamilton glass syringe at a rate of 150 $\mu\text{L h}^{-1}$ to prevent the formation of microbubbles. The needle was tapered and had an outer diameter at the end of approximately 200 μm . The working distance (WD) between the needle and substrate was set at 5 mm. As a predeposition nozzle treatment step, about 0.5 μL of solution was dispensed from the end of the needle to allow a thin coating of liquid to form on the outer surface of the nozzle. The resulting nozzle coating was allowed to dry for ~2 h to form a thin ChG film. The glass film was void of most solvent, which was removed with heat through a soft-bake process over a hot plate set at a surface temperature of 100 °C. This nozzle coating was

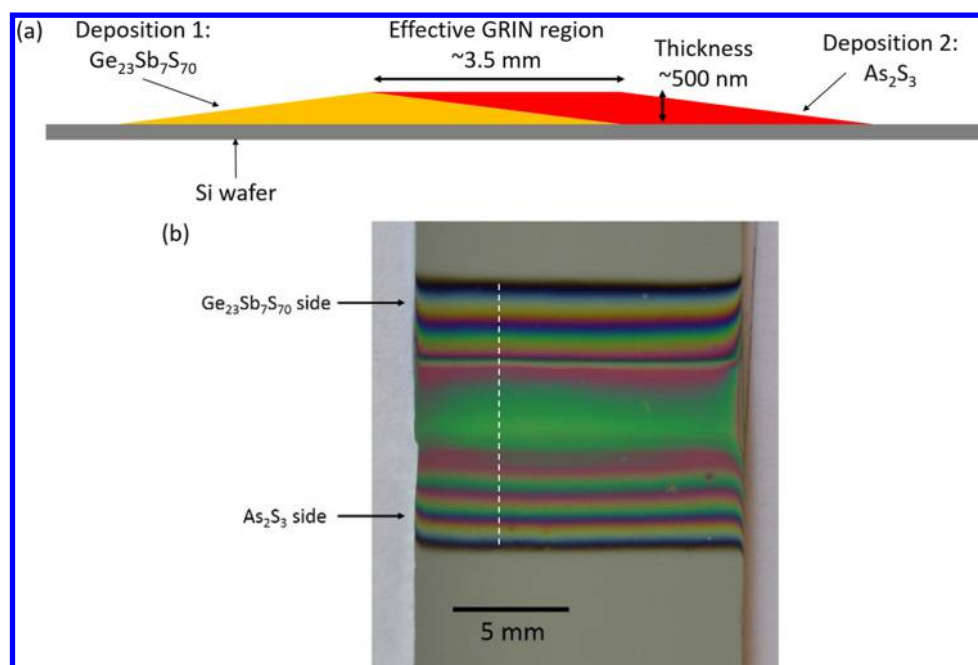


Figure 2. (a) Cross-sectional schematic and (b) photograph of a multilayer GRIN film, with the dashed line indicating the location of the thickness and refractive index profile in subsequent figures.

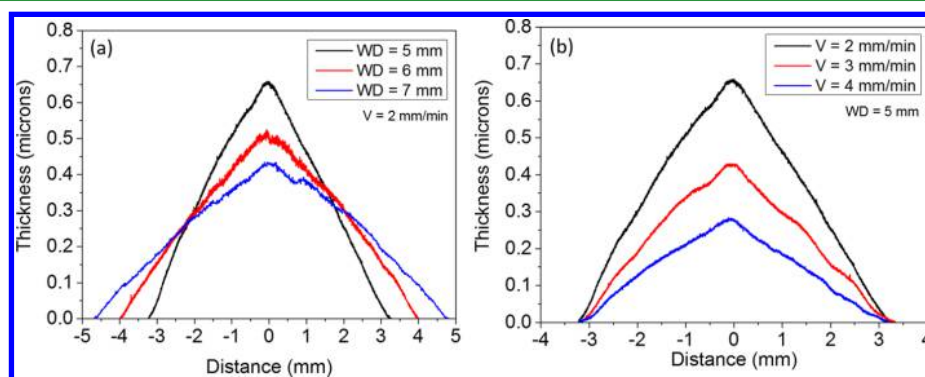


Figure 3. Variation in the $\text{Ge}_{23}\text{Sb}_7\text{S}_{70}$ film thickness profiles, measured normal to the one-dimensional motion of the spray nozzle: (a) variation of the WD; (b) variation of the nozzle translation velocity.

found to improve the stability of the spray by reducing the tendency for the ChG solution to wet the nozzle during deposition. Such coatings are an area of interest for continued optimization.

The hot-plate surface temperature was then set to 65 °C for the deposition of $\text{Ge}_{23}\text{Sb}_7\text{S}_{70}$, which promotes evolution of the solvent during deposition. Here, the solution flow rate was set at 10 $\mu\text{L h}^{-1}$, and the direct-current power was tuned until a stable Taylor cone was formed at approximately 3.5 kV. The $\text{Ge}_{23}\text{Sb}_7\text{S}_{70}$ layer was deposited on an ultraflat silicon wafer (Ted Pella product number 21610-6) by making 8 passes over the substrate in one dimension at a speed of 24 mm min^{-1} . The $\text{As}_{40}\text{S}_{60}$ layer was then deposited with motion parallel to the $\text{Ge}_{23}\text{Sb}_7\text{S}_{70}$ layer, approximately 4 mm apart, using 12 passes at a speed of 24 mm min^{-1} and a hot-plate surface temperature of 35 °C. Figure 2 shows a schematic representation of the resulting cross section of the GRIN film. This gradient bilayer film was then heat-treated under vacuum for 1 h each at 100 and 125 °C and 3 h at 150 °C to drive off residual solvent, resulting in a smooth, pinhole-free glass film.

Film thickness profiles were recorded with a Dektak XT contact profilometer. The surface roughness was measured in 50 locations across the bilayer film with a Zygo NewView 8300 white-light interferometer. Focused ion beam (FIB) was utilized to lift out a slice of the film for cross-sectional compositional analysis. In this process, a gold–palladium layer was first sputtered on the film to protect it from

reacting with the platinum layer, which is deposited during lift-out, preventing redeposition of the material removed by the FIB's gallium ion beam on the sample surface. The FIB slice was thinned to ~ 100 nm and imaged with transmission electron microscopy (TEM), and the composition profile was analyzed with energy-dispersive spectroscopy (EDS).

The lateral refractive index profile across the graded bilayer was measured at 1000 nm using mapping variable-angle spectroscopic ellipsometry (Woollam and Associates M2000), with a data fit using a lossy Cauchy model. Axial (depth) profiles could not be uniquely determined. The average refractive index at 1000 nm was determined at 25 points across the film with a 12 mm line scan and 0.5 mm spacing between the individual measurements by fitting the ellipsometry spectra with a lossy Cauchy model. The fitting error in the refractive index data was found to be less than 0.02 at all sampled locations. The ellipsometer's spot size at the sample surface was $\sim 100 \times 70 \mu\text{m}$, as determined by the system's focusing optics.

RESULTS AND DISCUSSION

The capability to print gradient thickness films is based on the inherent nature of ES to deposit ChG films of thickness dependent on several controllable variables, which may be nonuniform. Thus, it is incumbent that, prior to any deposition,

a complete assessment of the ES spray “spot” be precisely defined. The ES cone shape and resulting spray deposition spot geometry are dependent on various factors such as the nozzle geometry and deposition conditions.^{18,19} It was discovered that a linear motion of the spray (with needle oriented normal to the substrate surface) leads to films with approximately isosceles triangle thickness profiles, as shown in Figure 3.

Here the WD is varied while the spray movement speed (nozzle velocity, v) is fixed at 2 mm min^{-1} (Figure 3a), compared to measurements in part b, where the nozzle velocity is varied at a fixed WD of 5 mm.

The coverage area for the desired layer thickness profile is tuned by varying the WD of the spray, and the film thickness is controlled by the number of passes. Other variables critical to achieving a fixed index film layer include the solution flow rate, glass concentration within the solution and its resulting viscosity, and velocity of travel of the nozzle. Figure 4 shows

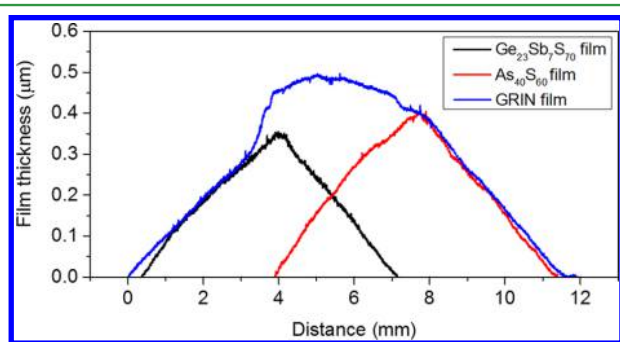


Figure 4. Individual film thickness profiles of $\text{Ge}_{23}\text{Sb}_7\text{S}_{70}$ and $\text{As}_{40}\text{S}_{60}$ and the resulting bilayer GRIN film thickness as a function of the spatial position. The peaks of the thickness profiles of the individual films are separated by 4 mm, the approximate distance between the films during fabrication of the GRIN film.

the individual thickness profiles of two independent, $\text{Ge}_{23}\text{Sb}_7\text{S}_{70}$ (black) and $\text{As}_{40}\text{S}_{60}$ (red), film layers, optimized to have approximately similar coverage area and thickness.

The blue line is the measured thickness profile of the resulting bilayer GRIN film. The measured thickness profile of the GRIN film matches that predicted based on an approximately uniform thickness region in the film's center, similar to the dashed line depicted in Figure 2b. The surface quality across the bilayer film was measured to range between 5 and 30 nm root-mean-square roughness, while the monolayer films were on the order of 5 nm.²⁰ Optimizing the surface quality is an area of future work.

Cross-sectional TEM was carried out to assess the film morphology uniformity and integrity (lack of voids) and to allow compositional verification as a function of the spatial position to confirm the chemical compositions associated with the resulting refractive index variation. The beam current was deliberately kept to a minimum to mitigate any possible beam-induced sample modification. Figure 5 illustrates a vertical cross-sectional image across the $\sim 0.5 \mu\text{m}$ bilayer film (a), showing the interface with both the underlying silicon substrate and the protective platinum overcoat.

There are no indications of voids or secondary phase formation such as phase separation or crystallization in this region from the center of the film. Figure 5b illustrates a compositional EDS spectrum taken from the center region of the film. This analysis was utilized to investigate the compositional variation of constituents with the film thickness. The spectrum clearly delineates the spatial variation of the unique constituents of the top ($\text{As}_{40}\text{S}_{60}$) layer arsenic, compared to the germanium found only in the underlying layer ($\text{Ge}_{23}\text{Sb}_7\text{S}_{70}$). Shown across the film thickness is the spatial variation of arsenic and germanium, as depicted by the relative color associated with each element, compared to the signature of the underlying substrate, silicon. While not quantitatively verified with chemical reference standards, the film's graded compositional variation of unique, individual layer constituents substantiates the clear intermixing of the two independently deposited layers.

In Figure 5b, the qualitative composition map was generated by the relative EDS peak heights of arsenic and germanium. No

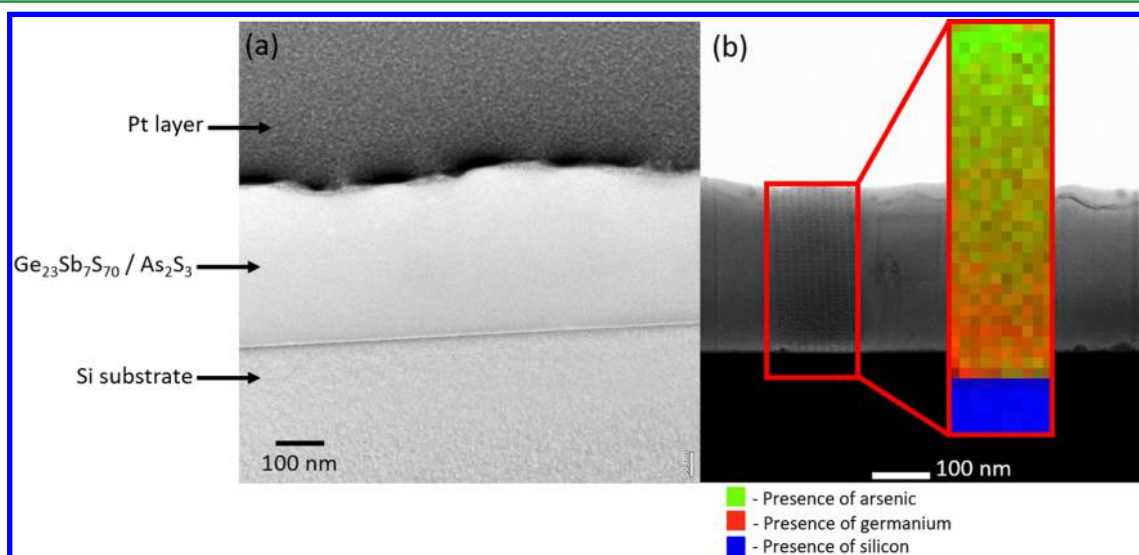


Figure 5. Cross-sectional TEM of an $\sim 100\text{-nm}$ -thick FIB lift-out specimen prepared from the center of the bilayer GRIN film shown in Figure 2a: (a) optical micrograph of the glass bilayer film on silicon, showing no interface between the two layers; (b) EDS analysis along the film thickness of the bilayer film showing dominant film constituents, where green represents the presence of arsenic, red represents the presence of germanium, and blue represents the presence of the substrate material, silicon.

distinct interface is seen in the TEM image, and the EDS data indicate a gradual change in composition along the film thickness. The mixing of the two layers is likely due to redissolution of the $\text{Ge}_{23}\text{Sb}_7\text{S}_{70}$ layer during the deposition of $\text{As}_{40}\text{S}_{60}$, and possibly diffusion, which may also occur during heat treatment of the multilayer film postdeposition. This phenomenon is considered beneficial because it is expected to lead to a smooth transition in the refractive index and thus reduces the possibility of Fresnel reflection losses in the device, which would be present in the case of a sharp compositional interface.

Spectroscopic ellipsometry was used to quantify the spatial variation in the average refractive index of the resulting film. Here, the average refractive index of the bilayer was probed by stepwise measurements across the film, maintaining spatial registration of the position to the thickness profile shown in Figure 4. Figure 6 shows the predicted refractive index at a wavelength of 1000 nm as a function of the position and the results of ellipsometry obtained by fitting the measured data with the lossy Cauchy model, demonstrating a significant

change in the refractive index (from 1.76 to 2.35) across the film.

The film thickness fit by the model matches fairly well with the thickness measured by profilometry, with the same basic shape and similar thickness at the overlapping region of the film, where thickness uniformity is expected. The position-dependent mean-square fitting error (MSE), not shown on this figure, indicates higher MSE in the center region, which is reasonable because of the intermixing of the layers. Also shown in Figure 6 is the refractive index profile predicted by a weighted average of the refractive index and thickness contributed by each electrospayed layer.

The magnitude of the index gradient Δn is ~ 0.4 over a relatively short distance of ~ 10 mm. A linear variation was targeted for the initial fabrication test, but this profile can theoretically be made arbitrary and the magnitude of the gradient ($\Delta n/\Delta \text{position}$) is only defined by the parent glass' indices and the programmed deposition profile. The agreement in the spatial variation of the bilayer film's compositional information combined with validation of the measured index variation conclusively illustrates the viability of ES to produce GRIN structures. As shown here, variation between the parent glass refractive indexes (2.21 and 1.88 respectively for As_2S_3 and $\text{Ge}_{23}\text{Sb}_7\text{S}_{70}$) suggests that the magnitude of the GRIN profile is only dependent on the ability to get target index glass compositions into solution. The slight offset of the bilayer film refractive index at the edges of the film to the monolayer films of each composition is attributed to process variation because the index of a solution-derived film depends on the amount of residual solvent. With the three films having been deposited and annealed separately, slight differences in the thermal profile are possible. Detailed studies on the relationship between the residual solvent and trends in the film refractive index compared to the corresponding bulk material can be found in the literature,^{16,17,21} and the electrospayed films in this study follow similar trends, with $\text{Ge}_{23}\text{Sb}_7\text{S}_{70}$ tending to remain below the bulk glass index and As_2S_3 tending to approach the bulk glass index. While demonstrated for multiple ChG compositions to date,²² removal of the residual solvent combined with the development of solvent-specific heat-treatment protocols when multiple glasses and additional layers are envisioned in more complex GRIN profiles will lead to an improvement in the final film optical quality. Additionally, further optimization of the flow rate uniformity to minimize abrupt variations in the index can further enhance the smoothness of the resulting index profile. Efforts to address complexities in correlating ES spray "spot" profiles to a desired index profile would be required to generate more complex, arbitrary GRIN profiles.

CONCLUSION

This study demonstrates a direct printing method for realizing multilayer IR-transparent GRIN coatings by an ES deposition process. This method could allow the generation of arbitrary GRIN profiles where the glass layer must be both physically and optically compatible with the underlying substrate. A GRIN with $\Delta n \sim 0.4$ (defined by the chosen parent glasses utilized) was realized. The GRIN fabricated by the deposition of individual controlled gradient thicknesses of $\text{Ge}_{23}\text{Sb}_7\text{S}_{70}$ and As_2S_3 films resulted in a profile closely matched to the target thickness profile. Bilayer film compositional variation was qualitatively correlated with the layer constituent content, and the lateral index and thickness variation showed agreement with predicted profiles based on ES spot coverage area calculations.

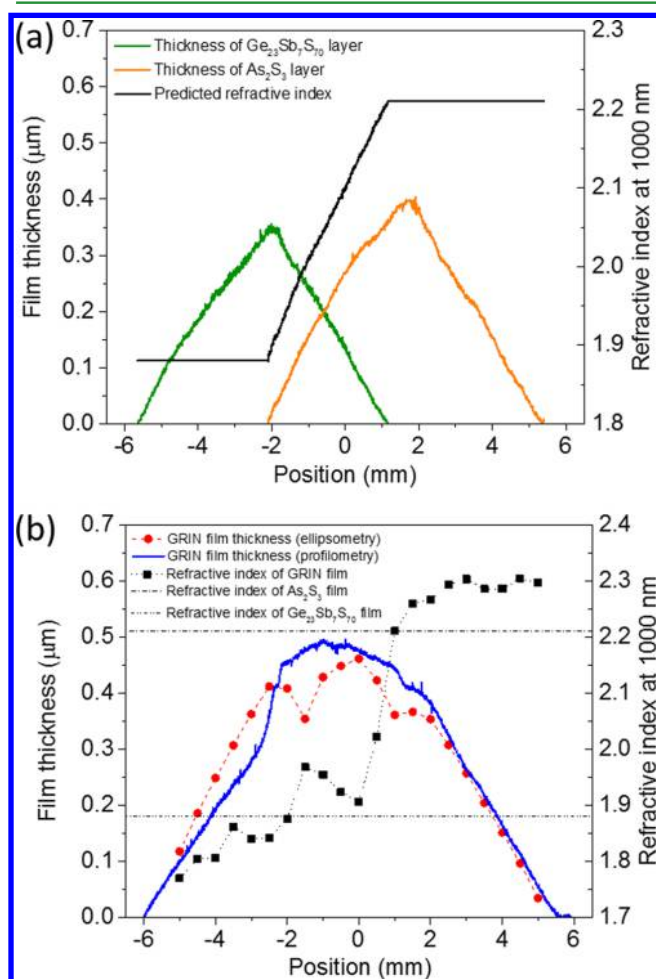


Figure 6. (a) Thickness profiles of individual films measured by contact profilometry and the predicted refractive index profile. Refractive index predicted by the weighted average of the film index and thickness from each electrospayed film. (b) Thickness and refractive index profiles of a bilayer GRIN film. The dashed lines on the refractive index and thickness measured by ellipsometry of the GRIN film are guides to the eye. Also shown are refractive index measurements of pure As_2S_3 and $\text{Ge}_{23}\text{Sb}_7\text{S}_{70}$ films deposited by ES.

These data suggest that some intermixing likely occurs at the bilayer interface during the deposition and/or heat-treatment process, resulting in a low loss gradient in composition. Because of the flexibility of ES, this method could theoretically be applied to various types of refractive index profiles, with simple tunability. With continued process development and optimization, this technique could be applied to the fabrication of microphotonics and bulk optical components.

AUTHOR INFORMATION

Corresponding Authors

*E-mail: spencen@g.clemson.edu.

*E-mail: kcr@creol.ucf.edu.

ORCID

Spencer Novak: 0000-0003-1754-2132

Pao Tai Lin: 0000-0002-5417-6920

Present Address

^SN.: LightPath Technologies, 2603 Challenger Tech Court, Suite 100, Orlando, FL 32826.

Author Contributions

The manuscript was written through contributions of all authors. All authors have given approval to the final version of the manuscript.

Notes

The authors declare no competing financial interest.

ACKNOWLEDGMENTS

This research was supported by the Defense Threat Reduction Agency (Grants HDTRA1-10-1-0073 and HDTRA1-13-1-0001) and National Science Foundation (Grant CMMI 1454406). The authors also acknowledge Matt Schneider of the Materials Characterization Facility, University of Central Florida, for TEM imaging.

REFERENCES

- (1) Yang, X. M.; Zhang, Y.; Syed. Infrared Waveguide Fabrications with an E-beam Evaporated Chalcogenide Glass Film. *J. Mod. Opt.* **2015**, *62* (7), 548–555.
- (2) Li, L.; Lin, H.; Qiao, S.; Zou, Y.; Danto, S.; Richardson, K.; Musgraves, J. D.; Lu, N.; Hu, J. Integrated Flexible Chalcogenide Glass Photonic Devices. *Nat. Photonics* **2014**, *8* (8), 643–649.
- (3) Charrier, J.; Brandily, M.-L.; Lhermite, H.; Michel, K.; Bureau, B.; Verger, F.; Nazabal, V. Evanescent Wave Optical Micro-sensor Based on Chalcogenide Glass. *Sens. Actuators, B* **2012**, *173*, 468–476.
- (4) Zha, Y.; Lin, P. T.; Kimerling, L.; Agarwal, A.; Arnold, C. B. Inverted-rib Chalcogenide Waveguides by Solution Process. *ACS Photonics* **2014**, *1* (3), 153–157.
- (5) Singh, V.; Lin, P. T.; Patel, N.; Lin, H.; Li, L.; Zou, Y.; Deng, F.; Ni, C.; Hu, J.; Giammarco, J.; Soliani, A. P.; Zdyrko, B.; Luzinov, I.; Novak, S.; Novak, J.; Wachtel, P.; Danto, S.; Musgraves, J. D.; Richardson, K.; Kimerling, L. C.; Agarwal, A. Mid-infrared Materials and Devices on a Si Platform for Optical Sensing. *Sci. Technol. Adv. Mater.* **2014**, *15* (1), 014603.
- (6) Hu, J.; Li, L.; Lin, H.; Zou, Y.; Du, Q.; Smith, C.; Novak, S.; Richardson, K.; Musgraves, J. D. Chalcogenide Glass Microphotonics: Stepping into the Spotlight. *Am. Ceram. Soc. Bull.* **2015**, *94* (4), 24–29.
- (7) Sun, Y.; Fan, X. Optical Ring Resonators for Biochemical and Chemical Sensing. *Anal. Bioanal. Chem.* **2011**, *399*, 205–211.
- (8) Yariv, A.; Yeh, P. *Optical Waves in Crystal: Propagation and Control of Laser Radiation*; John Wiley and Sons: New York, 1984.
- (9) Lin, P. T. Optical Materials and Devices for a Mid-IR Sensing Platform. *Proc. Adv. Photon. NT2C.2* **2015**, NT2C.2.
- (10) Kang, M.; Swisher, A. M.; Pogrebnjakov, A.; Liu, L.; Kirk, A.; Rivero-Baleine, C.; Smith, C.; Richardson, K.; Pantano, C. G.; Mayer,

T. S. Ultra-low Dispersion Multicomponent Thin Film Chalcogenide Glass for Broadband Gradient Index Optics. *ACS-Nano*. **2017**, submitted.

(11) Zhu, T.; Li, C.; Yang, W.; Zhao, X.; Wang, X.; Tang, C.; Mi, B.; Gao, Z.; Huang, W.; Deng, W. Electro Spray Dense Suspensions of TiO₂ Nanoparticles for Dye Sensitized Solar Cells. *Aerosol Sci. Technol.* **2013**, *47* (12), 1302–1309.

(12) Novak, S.; Johnston, D. E.; Li, C.; Deng, W.; Richardson, K. Deposition of Ge₂₃Sb₇S₇₀ Chalcogenide Glass Films by Electro spray. *Thin Solid Films* **2015**, *588*, 56–60.

(13) Novak, S.; Lin, P. T.; Li, C.; Borodinov, N.; Han, Z.; Monmeeyran, C.; Patel, N.; Du, Q.; Malinowski, M.; Fathpour, S.; Lumdee, C.; Xu, C.; Kik, P.; Deng, W.; Hu, J.; Agarwal, A.; Luzinov, I.; Richardson, K. Electro spray Deposition of Uniform Thickness Ge₂₃Sb₇S₇₀ and As₄₀S₆₀ Chalcogenide Glass Films. *J. Visualized Exp.* **2016**, *114*, e54379.

(14) Musgraves, J. D.; Wachtel, P.; Gleason, B.; Richardson, K. Raman Spectroscopic Analysis of the Ge-As-S Chalcogenide Glass-forming System. *J. Non-Cryst. Solids* **2014**, *386*, 61–66.

(15) Zou, Y.; Lin, H.; Ogbuu, O.; Li, L.; Danto, S.; Novak, S.; Novak, J.; Musgraves, J. D.; Richardson, K.; Hu, J. Effect of Annealing Conditions on the Physio-chemical Properties of Spin-coated As₂Se₃ Chalcogenide Glass Films. *Opt. Mater. Express* **2012**, *2* (12), 1723–1732.

(16) Waldmann, M.; Musgraves, J. D.; Richardson, K.; Arnold, C. B. Structural Properties of Solution processed Ge₂₃Sb₇S₇₀ Glass Materials. *J. Mater. Chem.* **2012**, *22* (34), 17848–17852.

(17) Novak, J.; Novak, S.; Dussauze, M.; Fargin, E.; Adamietz, F.; Musgraves, J. D.; Richardson, K. Evolution of the Structure and Properties of Solution-based Ge₂₃Sb₇S₇₀ Thin Films During Heat Treatment. *Mater. Res. Bull.* **2013**, *48* (3), 1250–1255.

(18) Cloupeau, M.; Prunet-Foch, B. Electrohydrodynamic Spraying Functioning Modes: a Critical Review. *J. Aerosol Sci.* **1994**, *25* (6), 1021–1036.

(19) Deng, W.; Klemic, J. F.; Li, X.; Reed, M. A.; Gomez, A. Increase of Electro spray Throughput Using Multiplexed Microfabricated Sources for the Scalable Generation of Monodisperse Droplets. *J. Aerosol Sci.* **2006**, *37* (6), 696–714.

(20) Novak, S. Electro spray Deposition of Chalcogenide Glass Films for Gradient Refractive Index and Quantum Dot Incorporation. Ph.D. Thesis, Clemson University, Clemson, SC, 2015.

(21) Song, S.; Dua, J.; Arnold, C. B. Influence of the Annealing Conditions on the Optical and Structural Properties of Spin-coated As₂S₃ Chalcogenide Glass Thin Film. *Opt. Express* **2010**, *18* (6), 5472–5480.

(22) Zou, Y. Novel Low-symmetry Gratings for Ultimate Light Trapping Enhancement in Next-generation Photovoltaics. Ph.D. Thesis, University of Delaware, Newark, DE, 2015.